Received 1 January 2006
Accepted 9 July 2006

A computational fluid dynamics analysis of a PEM fuel cell system for power generation

Elena Carcadea
National Research Institute for Isotopic & Cryogenic Technologies, Rm.Valcea, Romania
H. Ene
Mathematical Institute, Romanian Academy of Sciences, Bucharest, Romania
D.B. Ingham
Department of Applied Mathematics, University of Leeds, Leeds, UK
R. Lazar
National Research Institute for Isotopic & Cryogenic Technologies, Rm.Valcea, Romania
L. Ma and M. Pourkashanian
Centre for Computational Fluid Dynamics, University of Leeds, Leeds, UK, and
I. Stefanescu
National Research Institute for Isotopic & Cryogenic Technologies, Rm.Valcea, Romania

Abstract

Purpose – This paper aims to present a three-dimensional computational fluid dynamics (CFD) model that simulates the fluid flow, species transport and electric current flow in PEM fuel cells.

Design/methodology/approach – The model makes use of a general-purpose CFD software as a basic tool incorporating fuel cell specific submodels for multi-component species transport, electrochemical kinetics, water management and electric phase potential analysis in order to simulate various processes that occur in a PEM fuel cell.

Findings – Three dimensional results for the flow field, species transport, including waster formations, and electric current distributions are presented for two test flow configurations in the PEM fuel cell. For the two cases presented, reasonable predictions have been obtained, and this provides an insight into the effect of the flow designs to the operation of the fuel cell.

Research limitations/implications – It is appreciated that the CFD modeling of fuel cells is, in general, still facing significant challenges due to the limited understanding of the complex physical and chemical processes existing within the fuel cell. The model is now under further development to improve its capabilities and undergoing further validations.

Practical implications – The model simulations can provide detailed information on some of the key fluid dynamics, physical and chemical/electro-chemical processes that exist in fuel cells which are crucial for fuel cell design and optimization.

International Journal of Numerical Methods for Heat & Fluid Flow
Vol. 17 No. 3, 2007
pp. 302-312

0961-5539
DOI 10.1108/09615530710730166

One of the authors, Elena Carcadea would like to express her thanks to the University of Leeds and to the EU Marie Curie Fellowship scheme.

Originality/value – The model can be used to understand the operation of the fuel cell and provide and alternative to experimental investigations in order to improve the performance of the fuel cell.

Keywords Fluid dynamics, Fuels, Flow measurement

Paper type Research paper

Nomenclature

a = water vapor activity
c = molar concentration
D = species diffusivity
I = current density, A/m^2
j = current density, A/m^3
j_0 = exchange current density
p = pressure, atm
R = gas constant, 8.314 J/mol K
S = source terms
T = temperature
$\vec{u}$ = velocity vector, m/s
V = cell potential, V
Y = species mass fraction

Greek symbols
ε = porosity
η = overpotential, V
ϕ = phase potential, V
ρ = density, kg/m^3
μ = viscosity, kgm/s
σ = electric conductivity, S/m
λ = water content of the membrane

Superscript
eff = effective value
sat = saturation value

Subscripts
a = anode
c = cathode
e = electrolyte
i = species
ref = reference value

1. Introduction

The demand for a friendly environment and a reliable power source continues to increase at a rapid rate. One of the emerging technologies in power generation is the fuel cell technology. A fuel cell is an electrochemical device that converts the chemical energy of a fuel into electrical energy through chemical reaction instead of combustion. The high efficiency, high reliability and flexibility and ultra-low emission of the fuel cell makes it a strong candidate as an alternative power generation for both stationery and transportation applications. However, modeling of fuel cells still face substantial challenges and this is primarily due the our limited knowledge on various processes that occur in the fuel cell (Ma *et al.*, 2005). This paper presents a computational fluid dynamics (CFD) model that simulates the fluid flow, species transport and electric current flow in PEM fuel cells. The model simulations can provide detailed information on some of the key fluid dynamics, physical and chemical/electro-chemical processes that exist in fuel cells which are crucial for the optimization of fuel cells.

A basic PEM fuel can be made of three components, namely an anode that accommodates the fuel, a cathode that supplies oxidant, and an electrolyte which separates the anode and the cathode and provides a passage for the transport of ions. Both the anode and the cathode have three distinct components: the catalyst layer, the gas diffusion layer and the gas channel (Figure 1). The fuel and the oxidant are distributed through the gas channel to the diffusion layer across the fuel cell. The gas diffusion layer and the catalyst layer are made of porous materials so that the fuel and the oxidant can be further transported from the diffusion layer to the catalyst layer where electro-chemical reactions take place in order to generate electricity.

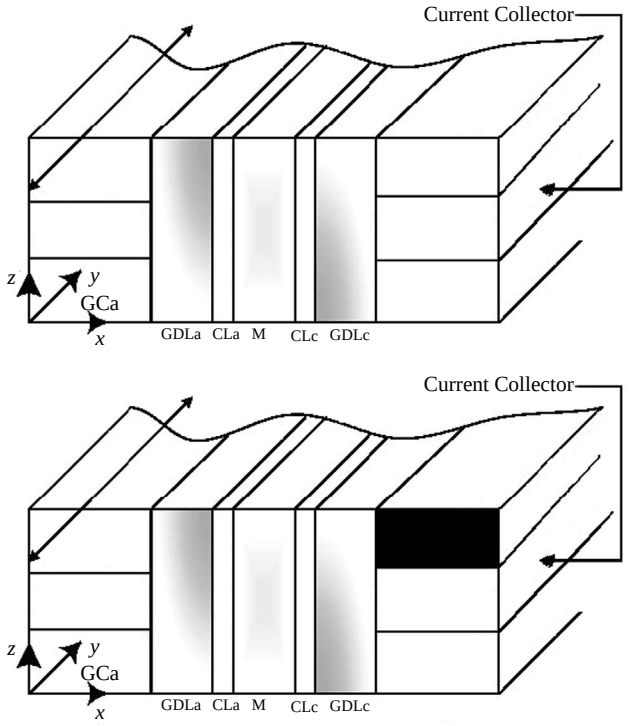

Figure 1.
The geometry of a fuel cell with straight channels (up), and interdigitated channels (down)

The purpose of the development of the CFD model is to numerically investigate various major physical and chemical processes that occur in the fuel cell, in particular, the effectiveness of the multi-component transport of the fuel and the oxidant across the fuel cell and its effects on the electrochemical kinetics and the overall performance of the fuel cell.

2. Model description

When developing the model, it is assumed that the fuel cell operates under steady and isothermal conditions, the fuel and the air flows can be treated as incompressible and laminar, and the porous media, such as the gas diffusion layer and the catalyst layers, are isotropic and homogeneous. Under these assumptions, the fluid flow, reactant species transport and the electrical potential in the fuel cell can be expressed by following conservative equations (Bernardi and Verbrugge, 1991):

$$\nabla \cdot (\varepsilon \rho \vec{u}) = 0 \tag{1}$$

$$\nabla \cdot (\varepsilon \rho \vec{u}\vec{u}) = -\varepsilon \nabla p + \nabla \cdot (\varepsilon \mu \nabla \vec{u}) + \mathrm{S}_u \tag{2}$$

$$\nabla \cdot (\varepsilon \vec{u} Y_i) = \nabla \left(D_i^{\mathrm{eff}} \nabla Y_i \right) + \mathrm{S}_i \tag{3}$$

$$\nabla \cdot \left(\sigma_{\mathrm{e}}^{\mathrm{eff}} \nabla \phi_{\mathrm{e}} \right) + \mathrm{S}_\phi = 0 \tag{4}$$

where $\vec{u}$, Y_i and ϕ_s denote the velocity vector of the fluid flow, the mass fraction of the ith species and the electric potential, respectively, within the fuel cell. For the fuel cell operated with hydrogen and air, typically four species may be considered in the system including hydrogen, H_2, oxygen, O_2, water, H_2O, and nitrogen, N_2. The source terms in equations (2–4) are due to the presence of the porous matrix, the chemical reactions and the ionization process.

The matrix of the porous elements of the fuel cell produces a significant resistance to the fluid flow. Typically this effect is modeled by the Darcy Law and this result in a momentum source in the momentum equation (2). Since, the resistance of the matrix is usually the dominant force in the flow system, the convective acceleration and the diffusion terms, appearing in equation (2), are relatively small and thus can often be ignored. However, it should be noted that the use of the Darcy law only has its limitations when modeling fluid flows in multi-component fuel cells when the porosities in different layers vary significantly and the Darcy law does not take into consideration the effect of the boundaries between the layers.

The consumption of the fuel and oxidant in the catalyst layers result in a concentration gradient across the fuel cell and the delivery of the reactants to the reaction site significantly rely on the process of species diffusion, which is primarily driven by the concentration gradients. The species diffusion transport is modeled in equation (3) with a species diffusivity coefficient. The presence of the porous matrix has a significant impact on the species diffusion and in this model this is modeled by employing the Bruggemann correction to the mass diffusivity coefficient as follows (Um and Wang, 2000):

$$D_i^{\text{eff}} = \varepsilon^{1.5} D_i \tag{5}$$

In this model we assume isotropic and homogenous porous media. It should be noted that in practice, due to the nature of the material of which the gas diffusion layer of the PEMFC is made, as well as the manufacturing process taken to make the fuel cell, the matrix is usually not isotropic and the pores are far from being homogenous.

Further, since at least three species are present in the system then the species transport in the fuel cell is a multi-component diffusive process in which the flux of one component is influenced by the concentration gradient of other components. The Maxwell-Stefan equations have been used to account for the cross-coupling between multi-species components and the binary mass diffusion coefficient are calculated using the following equation (Fuller and Newman, 1993):

$$\frac{\partial X_k}{\partial x^i} = \sum_{l=1}^{N} \frac{X_l X_m}{D_{lm}} \left(v_l^i - v_m^i\right) \tag{6}$$

where X is the species mole fraction, v denotes the component of the diffusive velocity of the species and D_{lm} is the binary diffusivity of any two species l and m.

The source term for the phase potential equation (4) only exits for the catalyst layer. This is because the ionization only takes place within the catalyst layer which produces the electric current. The transfer current densities are given by the Butler-Volmer equation (Um and Wang, 2000), as follows:

$$j_{\text{anode}} = j_{0,\text{a}}^{\text{ref}} \left(\frac{c_{\text{H}_2}}{c_{\text{H}_2}^{\text{ref}}} \right)^{1/2} \left[\exp\left(\frac{\alpha_{\text{a}} F}{RT} \, \eta_{\text{act,a}} \right) - \exp\left(-\frac{\alpha_{\text{c}} F}{RT} \, \eta_{\text{act,a}} \right) \right] \tag{7}$$

$$j_{\text{cathode}} = j_{0,\text{c}}^{\text{ref}} \left(\frac{c_{\text{O}_2}}{c_{\text{O}_2}^{\text{ref}}} \right) \left[\exp\left(\frac{\alpha_{\text{a}} F}{RT} \, \eta_{\text{act,c}} \right) - \exp\left(-\frac{\alpha_{\text{c}} F}{RT} \, \eta_{\text{act,c}} \right) \right] \tag{8}$$

where α_{a} and α_{c} are the transfer coefficients, $\eta_{\text{act,a}}$ and $\eta_{\text{act,c}}$ are the activation over-potential and $j_{0,\text{a}}^{\text{ref}}$ and $j_{0,\text{c}}^{\text{ref}}$ are the reference exchange current density at the anode and cathode side, respectively. The over-potentials should be a function of the transfer current density and in this model they are supplied as inputs into the model which, at the moment have to be obtained experimentally.

Water management is a critical issue for the performance of the PEM fuel cell since the polymer membrane must be in a highly hydrated state to facilitate proton transport. Water transport within the polymer membrane is controlled by two, usually opposite processes, namely the electro-osmotic drag and the back diffusion. When the PEMFC is in operation, hydrogen ions moving through the electrolyte from the anode to the cathode pull the water molecules with them. The larger the number of ions transferred then the more water will be dragged along with them. Thus, the water content in the electrode is determined by both the water generation due to the oxygen reduction reaction and the water flux to/from the polymer membrane. In the model presented, the molar flux of water, α, is calculated based on the electro-osmotic drag coefficient n_{d}, water content, λ, and water activity, a, and these values are given by the following expressions (Bernardi and Verbrugge, 1991; Fuller and Newman, 1993; Nguyen and White, 1993):

$$\alpha = \frac{n_{\text{d}} \cdot j}{F} \tag{9}$$

$$n_{\text{d}} = 0.0028\lambda + 0.05\lambda - 3.5 \times 10^{-19} \tag{10}$$

$$\lambda = \begin{cases} 0.043 + 17.18a - 39.85a^2 + 36.0a^3 & \text{for } 0 < a \leq 1 \\ 14 + 1.4(a - 1) & \text{for } 1 \leq a \leq 3 \end{cases} \tag{11}$$

$$a = \frac{X_{\text{H}_2\text{O}} p}{p^{\text{sat}}} \tag{12}$$

$$\begin{aligned} \log_{10} p^{\text{sat}} = {} & -2.1794 + 0.02953(T - 273.15) - 9.1837 \times 10^{-5}(T - 273.15)^2 \\ & + 1.4454 \times 10^{-7}(T - 273.15)^3 \end{aligned} \tag{13}$$

A summary of the source terms in equations (2)-(4) is given in Table I. In order to solve the governing set of equations (1)-(4) incorporating the supplementary equations (5)-(13), we employed a single computational domain that covers every component of the fuel cell. As a result, no condition at the interface between the different components of the fuel cell is required, except that a special treatment is implemented for equation (4) where a no-flux of electrons has been assumed across the membrane. Boundary conditions are only required at the external surfaces of the fuel cell and typically they

include the fluid flow conditions at the inlets and outlets of the gas channels and the operational potential of the fuel cell.

As a preliminary test of the model, we have used a straight channel fuel cell unit (Um and Wang, 2000) (Figure 1). It consists of an anode and a cathode sandwiched with a polymer electrolyte. Within each electrode there are two parallel straight gas channels, a gas diffusion layer and a very thin catalyst layer. Porous graphite has been used to support the electrodes and act as a current collector. In the simulation, two types of flow configurations have been investigated, namely, the straight flow configuration and the interdigitated flow configuration. In both configurations co-flow arrangements have been used, i.e. the fuel and air are fed in from the same end and flow in the same direction in the fuel cell. The interdigitated flow configuration is formed by injecting the air into the bottom channel from one end and forcing it out from the top channel at the other end. The other end of the channels are blocked (Figure 1(b)).

Figure 2 shows a typical computational domain that has been employed with a coarse grid consisting of about 106,000 cells. A finer grid has been tested which consists of about 530,000 computational cells and the results obtained are graphically indistinguishable between the two meshes. Since, the Reynolds number of the fluid flow in the fuel cell is very small, a laminar flow is assumed throughout the cell. The phase potential is set to be zero on the anode side and a constant value on the cathode side. The rates of fuel and air flows have been specified at the inlets of the gas channels and at the outlets a pressure condition has been specified. The details of the physical and operational parameters employed are listed in Table II.

Governing equations	Volumetric source terms
Momentum transport	$S_u = -(\mu/k)\varepsilon u$
Hydrogen transport (anode)	$S_{H_2} = -(M_{H_2}/2F)\cdot j_{anode}$
Oxygen transport (cathode)	$S_{O_2} = -(M_{O_2}/4F)\cdot j_{cathode}$
Water transport (anode)	$S_{H_2O} = -M_{H_2O}\cdot\alpha$
Water transport (cathode)	$S_{H_2O} = M_{H_2O}\cdot\alpha + (M_{H_2O}/2F)\cdot j_{cathode}$
Phase potential	$S_\phi = -j$

Table I.
Source terms of conservation equations

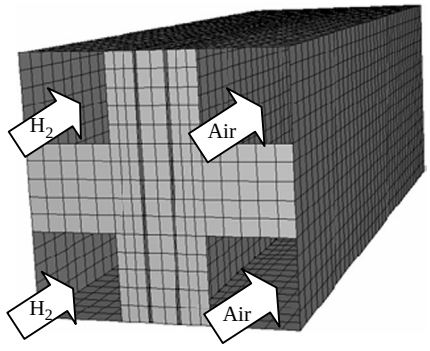

Figure 2.
Computational domain with a coarse grid

Property	Value	
Cell length (cm)	7.112	
Gas channel height (cm)	0.0762	
Gas channel width (cm)	0.0762	
Current collector width (cm)	0.0762	
Anode/cathode GDL thickness (cm)	0.0254	
Membrane thickness (cm)	0.0178	
Anode catalyst layer thickness	0.001 cm	
Cathode catalyst layer thickness	0.001 cm	
Porosity of GDL	0.8	
Porosity of CL	0.4	
Cell temperature (K)	353	
Inlet N_2/O_2 mole fraction ratio	0.79/0.21	
Pressure at the anode/cathode gas channel	3/5 (atm)	
	Anode	*Cathode*
Velocity(m/s)	0.5	0.35
Mass fraction of H_2	0.406	0
Mass fraction of H_2O	0.594	0.08534
Mass fraction of O_2	0	0.23
Inlet temperature (K)	353	353

Table II.
Physical and operating parameters

3. Results and discussions

Because the length of the cell (in the *y*-direction) is very large compared with the other dimensions of the cell, we have scaled the *y*-direction with a factor 0.1 for all the figures presented, in order to achieve a good visualization of the results.

Figure 3 shows the velocity contours in two representative planes within the gas channels and across the diffusion layers for both straight and interdigitated configurations. It can be seen that for the straight channel configuration, Figure 3(a), in the anode side the velocity is maximum at the inlet and gradually decreases along the flow channel due to the effect of flowing into the diffusion layer and the consumption of the fuel. A slight increase in the flow speed may be observed near to the exit. In the cathode side, an increase in the gas velocity may be observed due to the formation of water that increases the mass flow rates of the flow. Fluid velocities within the porous regions are generally very small compared to that in the gas channel. Further, significant secondary flows are observed both in the gas channel and across the porous regions. For the interdigitated configuration, Figure 3(b), in the cathode side the fluid velocity are very small at the dead ends of both the upper and the bottom channels while high speed flows appear at the inlet and out let of the channel. The air is forced to penetrate the porous current collector between the lower and the upper channels and this is beneficial to an efficient delivery of the oxygen across the region.

Figure 4 shows the distribution of oxygen in the fuel cell in terms of mass fractions. The contours of oxygen mass fractions are shown in a reaction surface within the catalyst layer and two sections across the gas channels in the cathode side for the straight flow configuration, Figure 4(a), and for the interdigitated flow configuration, Figure 4(b). In both configurations, air flow is coming in form the left hand side and discharged from the right hand side of the channel. The concentration of the oxygen is decreasing downstream of the channel for both cases due to

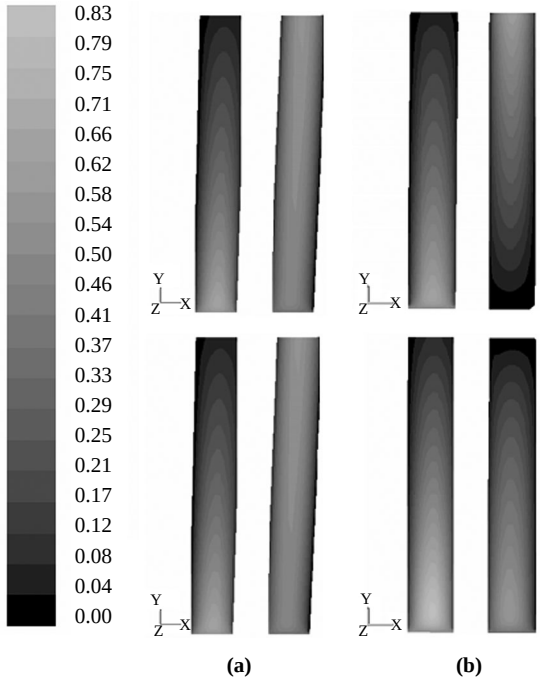

Figure 3.
Velocity contours above/under current collector for a cell with: (a) straight and (b) interdigitated fuel channels

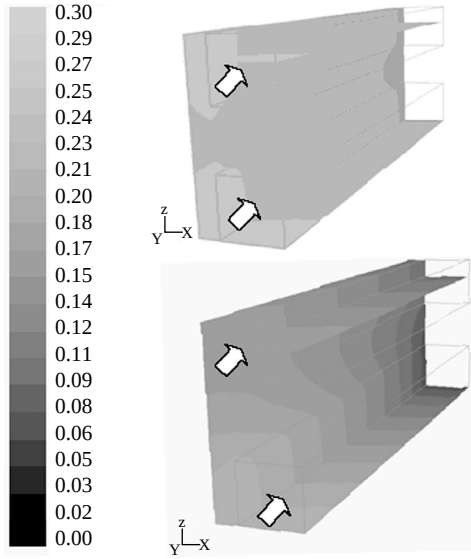

Figure 4.
The O_2 mass fraction for a cell with: straight fuel channels (up), interdigitated fuel channels (down)

chemical/electrochemical reactions that consume oxygen. In the case of the straight channel, the oxygen decreases monotonically along the gas channels as the electrochemical reaction proceeds and the profile of oxygen concentration shows a symmetrical pattern about the *z*-axis due to the symmetrical flow arrangement. It is noted that due to the effect of the porous current collector, a low oxygen concentration regions exists underneath the current collector around the axis of symmetry. Under a straight flow configuration, the convective flow is in parallel to the gas channel and the oxygen delivery to the region covered by the current collector is mainly through diffusion processes and this substantially limits the efficient delivery of the reactants to the reaction site. However, this situation may be changed by using the interdigitated flow configuration, Figure 4(b), where the air is forced to flow through the porous current collector before it discharged at the top channel. As we can observe in Figure 4 that the overall distribution of the oxygen in the interdigitated flow configuration is very different from the case in the straight flow configuration. Oxygen concentration in the region underneath the current collector is improved significantly and lowest oxygen concentration is near to the dead end of the bottom air channel. The dead zone formed at the end of the channel limits the transfer of the oxygen to the region.

The change in the air delivery between the two flow configurations has a significant impact on the performance of the fuel cell. Figure 5 shows the predicted cathode side electrical potentials in a plane within the catalytic reaction layer. For the straight flow configuration, Figure 5(a), the profile of the phase potential is symmetric and the maximum phase potential occurs at the inlet of the channel, where the highest oxygen concentration exists. Downstream of the channel the potential decreases with the

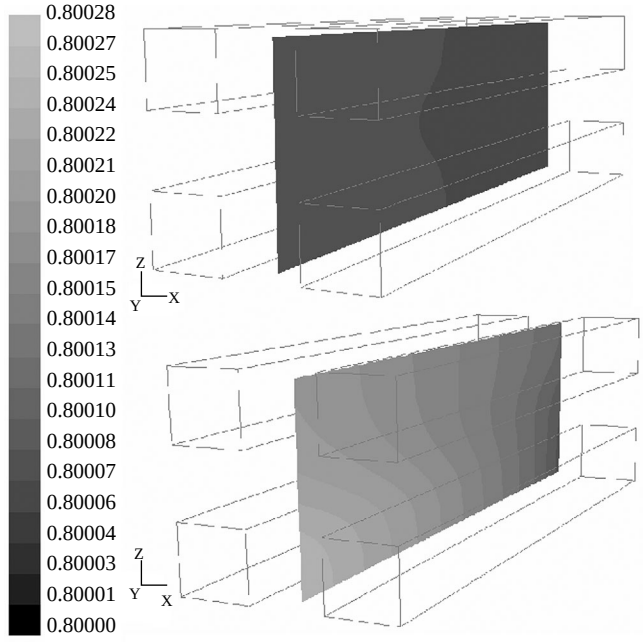

Figure 5.
The phase potential profiles for the cell with: straight fuel channel (up), interdigitated fuel channel (down)

decrease in the oxygen supply in the gas stream. The lowest potential occurs in the region covered by the current collector. In the case of interdigitated flow (Figure 5(b)), oxygen supply in the region improves and thus the phase potential. In general, a relatively higher phase potential is predicted for the interdigitated flow configuration compared to the straight flow configuration.

In order to keep the polymer electrolyte active, moisture is usually introduced in the fuel gas flow to compensate the water losses due to the electro-osmotic action in the electrolyte. The predicted water transportation in the anode and the cathode of the fuel cell are shown in Figure 6. In the anode side, the water concentration steadily decreases along the gas flow while in the cathode it increases due to the water production in the reaction and the influx of water from the electrolyte. At the exit of the gas channel on the cathode side of the interdigitated flow configuration, Figure 6(b), the gas flow contains more water than it does in the straight flow configuration, Figure 6(a), showing an improve performance of the fuel cell. It should be noted that in some situations water back diffusion from the cathode to the anode may occur if the water content at the cathode is much higher than it is at the anode side, particularly when a low ionization-efficiency exists downstream of the gas flow channel. It should also be noted that liquid water may form if the water partial pressure is higher than the saturated vapor pressure. The existence of the liquid water in the catalyst and the gas diffusion layers can block the effective reacting surface and the pores of the diffusion layer. In this situation, employing a single-phase flow model will be inaccurate.

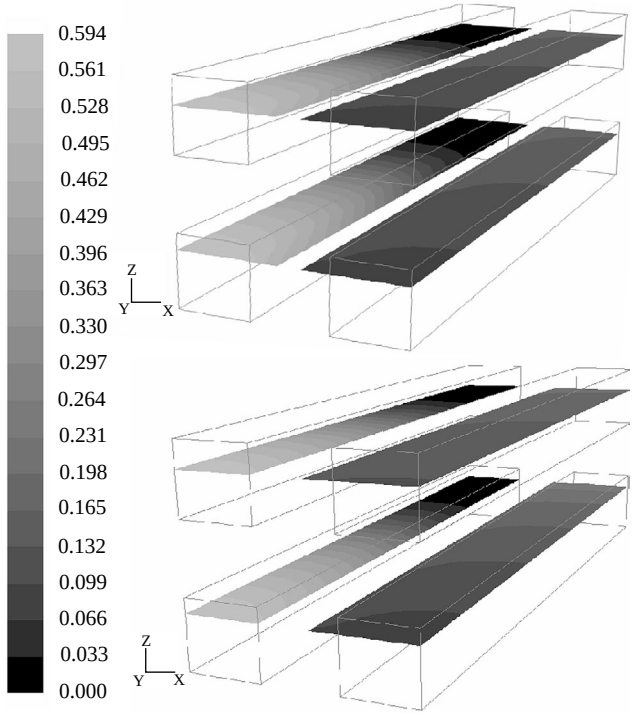

Figure 6.
Water mole fraction profile for a cell with: straight fuel channels (up), interdigitated fuel channels (down)

4. Conclusions

This paper presents results from a three-dimensional, steady state, single-phase model of a PEM fuel cell that has been developed using the fluent CFD software as a basic tool. The fuel cell specific sub-models have been developed which incorporate the electrochemical kinetics and multi-dimensional fluid flow and multi-component species transport. Water management and electric fields under typical PEMFC operation conditions have been simulated. For the two test cases presented, reasonable predictions have been obtained for both the reactant distributions, including water formations across the cell as well as the cell potentials predictions. The model is now under further development to improve its capabilities and under going further validations. It is appreciated that the CFD modeling of fuel cells is, in general, still facing significant challenges due to the limited understanding of the complex physical and chemical processes existing within the fuel cell. However, with the further development of the modeling capabilities, the modeling of fuel cells using CFD techniques can be an important alternative to the experimental measurements in providing information that is critical to the fuel cell design and optimization.

References

Bernardi, D. and Verbrugge, M.W. (1991), "A mathematical model of the solid-polymer-electrolyte fuel cell", *J. Electrochem. Society*, Vol. 139 No. 9, p. 2477.

Fuller, T.F. and Newman, J. (1993), "Water and thermal management in solid-polymer-electrolyte fuel cells", *J. Electrochem. Society*, Vol. 140, pp. 1218-25.

Ma, L., Ingham, D.B., Pourkashanian, M.C. and Carcadea, E. (2005), "Review of the computational fluid dynamics modeling of fuel cells", *Journal of Fuel Cell Science and Technology*, Vol. 2 No. 4, pp. 246-57.

Nguyen, T.V. and White, R.E. (1993), "A water and thermal management model for proton exchange membrane fuel cells", *J. Electrochem. Society*, Vol. 140, pp. 2178-86.

Um, S. and Wang, C.Y. (2000), "Computational fluid dynamics modeling of proton exchange-membrane fuel cells", *J. Electrochem. Society*, Vol. 147, pp. 4485-93.

Corresponding author

D.B. Ingham can be contacted at: D.B.Ingham@leeds.ac.uk; amt6dbi@amsta.leeds.ac.uk